agriculture

MDPI

Article

Widely Targeted Metabolomics Analyses Clarify the Biosynthetic Pathways Responsible for Flavonoids in Sweet Potato (*Ipomoea batatas* (L.) Lam.) Storage Roots

Huiyu Gao [1], Yuyang Zhang [1], Qian Duan [1], Qingming Ren [1], Lin Deng [1], Yiqiong Huo [1], Bin Zhang [1,2,*] and Xiaoxi Zhen [3,*]

[1] College of Agriculture, Shanxi Agricultural University, Jinzhong 030801, China; s20212162@stu.sxau.edu.cn (H.G.); s20222109@stu.sxau.edu.cn (Y.Z.)
[2] Institute of Agricultural Bioengineering, Shanxi Agricultural University, Jinzhong 030801, China
[3] Shanxi Key Laboratory of Minor Crop Germplasm Innovation and Molecular Breeding, Shanxi Agricultural University, Taiyuan 030031, China
* Correspondence: binzhang@sxau.edu.cn (B.Z.); xiaoxizhen@sxau.edu.cn (X.Z.)

Abstract: Sweet potatoes (*Ipomoea batatas* (L.) Lam.) are a widely cultivated member of the Convolvulaceae family. Despite intensive agricultural interest, the metabolic determinants of sweet potato quality remain poorly understood owing to a lack of reliable or systematic sweet potato metabolite analyses. This study aimed to reveal the mechanism of flavonoid biosynthesis using widely targeted metabolomics and qRT-PCR analysis of white (S19) and yellow (BS) sweet potatoes. We found that the *PAL*, *C4H*, *4CL*, *CHS*, *CHI*, *IFS*, *F3H*, *F3′H*, *DFR*, *ANS*, and *ANR* genes were differentially expressed in BS. Upregulation of *PAL*, *C4H*, *4CL*, and *CHS* led to the accumulation of large amounts of chalcone, which is highly expressed in yellow flesh, resulting in the yellow color of BS. In S19, the high expression of *FLS* and the low expression of *DFR* inhibited pigment accumulation, while the low expression of *CHS* also inhibited flavonoid synthesis, ultimately leading to the white color. In conclusion, this study identified the main differentially expressed genes and their metabolites in the flavonoid biosynthesis pathway, and preliminarily elucidated the mechanism underlying the different flesh colors in sweet potato, thus providing new insights into the composition and abundance of metabolites in sweet potatoes with different-colored flesh.

Keywords: flavonoid biosynthesis; metabolome; sweet potato

Citation: Gao, H.; Zhang, Y.; Duan, Q.; Ren, Q.; Deng, L.; Huo, Y.; Zhang, B.; Zhen, X. Widely Targeted Metabolomics Analyses Clarify the Biosynthetic Pathways Responsible for Flavonoids in Sweet Potato (*Ipomoea batatas* (L.) Lam.) Storage Roots. *Agriculture* **2023**, *13*, 1955. https://doi.org/10.3390/agriculture13101955

Academic Editor: Fabio Sciubba

Received: 31 August 2023
Revised: 4 October 2023
Accepted: 6 October 2023
Published: 7 October 2023

1. Introduction

Sweet potato (*Ipomoea batatas* (L.) Lam.) is a dicotyledonous vegetable belonging to the Convolvulaceae family. It ranks seventh in the list of the most produced crops in the world following wheat, rice, maize, potato, barley, and cassava [1]. Previous studies have shown that sweet potato is rich in anthocyanins, carotene, flavonoids, and other active ingredients, with the advantages of being tasty and healthy, together with having medicinal functions [2,3]. Therefore, the study of flavonoid biosynthesis in sweet potato is of great significance for quality improvement.

Flavonoids are major secondary metabolites, and consist of two benzene rings and pyran rings. Flavonoids can be classified into seven categories based on the structure of the pyran rings, namely, flavonoids, flavonols, flavanones, anthocyanins, isoflavones, and proanthocyanidins [4]. Several different structural genes have been identified as regulators of flavonoid biosynthesis in species including Arabidopsis [5], rice [6], and maize [7]. This complex biosynthetic process incorporates the general phenylpropane pathway [8], with phenylalanine ammonia lyase (PAL), cinnamic acid 4-hydroxylase (C4H), and 4-Coumariinyl-CoA ligase(4CL), converting phenylalanine into *p*-Coumaroyl-CoA,

whereafter chalcone synthase (CHS) and chalcone isomerase (CHI) can, respectively, produce naringenin chalcone and flavanone [9]. Next, Flavanone 3-/flavone 3′-/flavone 3′5′-hydroxylase (F3H/F3′H/F3′5′H) generate dihydroflavonol, which is processed by flavonol synthase (FLS) in the context of flavonol biosynthesis [10]. Dihydroflavonol reductase (DFR) and anthocyanin synthase (ANS) can also, respectively, reduce and oxidize dihydroflavonol to yield leucoanthocyanins and anthocyanins, with NADPH participating in the former process [11]. Proanthocyanidins are additionally generated from leucoanthocyanins and anthocyanins through the activity of leucoanthocyanidin reductase (LAR) and anthocyanin reductase (ANR) [12].

Flavonoids are commonly found in plants, where they play vital roles in many biological processes such as plant growth and development, resistance to biotic and abiotic stresses, and interactions with other organisms [13]. The expression levels of the flavonoid-related genes *F3H*, *DFR*, *ANS*, and *F3′H* were found to be significantly increased in corn grains under light conditions, thus improving the corn quality [14]. In addition, flavonoids play important roles in drought tolerance, and the expression of *CHS*, *CHI*, *F3H*, *FLS*, and *DFR* has been found to differ significantly in conditions of drought stress [15]. The antioxidant capacities of red and black rice are significantly higher than that of white rice, which is caused by the higher contents of total flavonoids [16].

Plants produce abundant quantities of metabolites that vary in both structure and function. These metabolites play important roles in plant growth and development and in coping with environmental stress, and also form chemical basis variations in crop yield and quality [17]. Continuous advances in technology have seen the gradual development of targeted metabolomics into widely targeted metabolomics. Metabolomics strategies are widely used in the analysis of spatiotemporal metabolism during plant development [18]. Yang et al. [19] used widely targeted metabolomics to evaluate the metabolites of golden buckwheat and identified the key metabolites. Using widely targeted metabolomics and transcriptomics, the effects of NOR-like1 transcription factors on the accumulation of alkaloids, phenolic acids, and flavonoids in tomato at different maturation stages were preliminarily determined, laying a foundation for extending the shelf life of the fruit and the cultivation of resistant plants [20]. Wang A [21] et al. used Liquid Chromatography–Electrospray Ionization–Mass Spectrometry to analyze the metabolic profiles of five sweet potato cultivars exhibiting different flesh colors, providing new insights into the differences in metabolite profiles among sweet potatoes with different flesh colors.

There have been few metabolic or molecular studies conducted to date focused on the characterization of sweet potato flavonoid profiles. As such, a widely targeted metabolomics approach was herein used to quantify and compare the abundance of flavonoid metabolites and flavor-related compounds in sweet potato storage roots from the white-fleshed S19 and yellow-fleshed BS cultivars. Molecular analyses of metabolite biosynthesis-associated genes were also performed with the goal of better clarifying the molecular drivers of sweet potato flavonoid biosynthesis

2. Materials and Methods

2.1. Plant Materials

This study utilized the white-fleshed Shangshu 19 (S19) and yellow-fleshed Baishu (BS) sweet potato cultivars, which were planted on 30 May 2021 in a Shanxi Agricultural University experimental farm (112.58′ E, 37.42′ N). Fresh root samples were harvested on day 90 (S1), day 100 (S2), day 110 (S3) and day 120 (S4) after planting. Storage roots of similar size with a smooth epidermis were utilized for further characterization and stored at −80 °C.

2.2. Sample Preparation and Extraction

Sweet potato storage root samples were freeze-dried using a Scientz-100F vacuum freeze-dryer (Ningbo, China) and ground (30 Hz, 1.5 min) to produce a lyophilized powder using zirconium beads (MM 400, Retsch, Haan, Germany). Then, 100 mg of the lyophilized

samples were lysed in a 1.2 mL volume of 70% methanol, centrifuging the samples for 30 s every 30 min and repeating this process six times in total. The resultant samples were then stored overnight at 4 °C, centrifuged (12,000 rpm, 10 min), and used for UPLC-MS/MS analyses. To prepare quality control (QC) samples, aliquots of each sample were mixed together. To ensure measurement reproducibility, these QC samples were analyzed after every six samples during UPLC analyses [22–27].

2.3. Measurement of Flavonoid Levels in Sweet Potato Storage Roots

2.3.1. Rutin Standard Curve Preparation

Referring to Yang et al.'s method [28], initially, 20 mg of the rutin standard was mixed with 60% ethanol, and dissolved in a water bath at a temperature lower than 60 °C. The above mixture was then added to a 100 mL volumetric flask, allowed to cool, and set aside while preparing a 0.2 g/L rutin standard solution. Then, 10 mL volumetric flasks were filled with a range of rutin standard volumes (0, 0.4, 0.8, 1.2, 1.6, 2.0, or 2.4 mL). The aluminum nitrate method was used to establish a linear regression equation for these standard samples.

Briefly, 7.4 mL of the appropriate rutin standard solution was added to a 10 mL flask. Then, 0.3 mL of 5% sodium nitrite was added. These samples were shaken thoroughly for 4 min, and 0.3 mL of 10% aluminum nitrate was added. After shaking for an additional 4 min, 2 mL of 4% sodium hydroxide was mixed into the solution. Sample volumes were then adjusted to 10 mL using 60% ethanol, and these solutions were shaken thoroughly before being left to stand for 12 min. A blank control sample was also prepared in parallel. Within 3 min of this step, 300 µL of each sample was aliquoted to a 96-well plate, and absorbance at 510 nm was measured using a microplate reader (Figure 1).

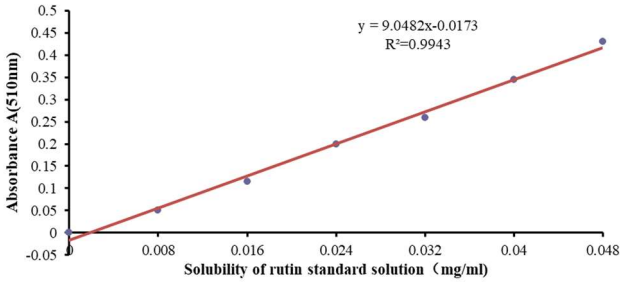

Figure 1. Rutin standard curve.

2.3.2. Analysis of Flavonoid Content

After removing samples (S1–S4) from storage at −80 °C, they were freeze-dried for 48 h, followed by storage at −20 °C. Then, 0.25 g of lyophilized powder from each sample was added into a 50 mL tube and mixed thoroughly with 60% ethanol. Following ultrasonication for 20 min, samples were ultrasonicated for 40 min and centrifuged (12,000 rpm, 10 min), and 7.4 mL of the supernatant was placed in a 10 mL flask followed by the dropwise addition of 5% sodium nitrite (0.3 mL). After thoroughly mixing these samples, they were allowed to stand for 4 min. Next, 0.3 mL of 10% aluminum nitrite was added, and they were allowed to stand for 4 min after mixing, with subsequent 4% sodium hydroxide addition (2 mL). These samples were then mixed via repeated inversion and allowed to stand for 12 min. Finally, 300 µL of the liquid fraction was collected and absorbance at 510 nm was measured, with the total flavonoid contents in the 10 mL samples then being computed as follows:

$$\begin{aligned} E = CNV/m &= (0.1105X + 0.0019) \times N \times V/m \\ &= (0.1105X + 0.0019) \times (10/7.4) \times 10/0.25 \\ &= (0.1105X + 0.0019) \times 54.0541 = 5.9730 \times A + 0.1027 \end{aligned}$$

E: Extraction rate (mg/g).
N: The dilution factor for the extraction solution.
C: Corrected flavonoid concentration (mg/mL).
V: Extract volume (mL).
M: Sample mass (g).

2.4. UPLC Analyses

Fresh root samples (S2 and S4) were selected for widely targeted metabolomics analyses and the recording of phenotypic characteristics. Extracted samples were analyzed using a UPLC-ESI-MS/MS system (UPLC: SHIMADZU Nexera X2; MS: Applied Biosystems 4500 Q TRAP) with an Agilent SB-C18 (1.8 µm, 2.1 mm × 100 mm) column and a mobile phase consisting of 0.1% formic acid in water (A) and 0.1% formic acid in acetonitrile (B). The linear gradient settings were as follows: the concentration was gradually increased to 5% A and 95% B over 9 min, followed by the maintenance of this 5% A and 95% B concentration for 1 min, with a gradual shift to 95% A and 5% B over a 1.10 min interval, followed by the maintenance of this latter combination for 2.9 min. A 0.35 mL/min flow rate and a 40 °C column temperature were used throughout this process, and the sample injection volume was 4 µL. The effluent was used for ESI–triple quadrupole-linear ion trap (Q-TRAP)–mass spectrometer analyses, as detailed previously [22–27].

2.5. ESI-Q TRAP-MS/MS

Linear ion trap (LIT) and triple quadrupole (QQQ) scanning were performed via a Q-TRAP approach under the control of Analyst 1.6.3 (AB Sciex). An AB4500 Q TRAP UPLC/MS/MS system with an ESI turbo ionization source was operated in positive/negative ion modes (ESI+/ESI−) using the following settings: turbojet ion source; source temperature = 550 °C; ion injection voltage (IS) = 5500 V (ESI+)/−4500 V (ESI−); ion source gas I (GSI), gas II (GSII), and respective curtain gas (CUR) pressures of 50 psi, 60 psi, and 25.0 psi. The optimization of these settings and QC analyses were performed in LIT and QQQ modes with polypropylene glycol (PLG) solution (10 and 100 µM). QQQ scan results were obtained through multiple reaction monitoring (MRM), adjusting the use of nitrogen as the collision gas. Additional Declustering Potential (DP) and Collision Energy (CE) optimization were used for individual MRM conversions, with unique MRM conversions being monitored based on the metabolites eluted during different points in time [22–27].

2.6. Metabolite Quantification and Characterization

When analytical standards were available for purchase (Sigma-Aldrich, St. Louis, MI, USA), preliminary and complementary MS data analyses were performed based on comparisons of the precursor ion (Q1) and product ion (Q3) values, retention times, and fractionation modes to those of the control samples. When standards were unavailable, data were analyzed using the MWDB database produced by MetWare Biological Science and Technology Co., Ltd. (Wuhan, China), and other metabolite database resources available for analysis. K^+, Na^+, $NH4^+$, and other high-molecular-weight ions were excluded during the identification process, and duplicate signatures were avoided.

Quantitative analyses were conducted in MRM mode. Briefly, the signal intensity for each metabolite was assessed through the selective identification of QQQ MS signature ions. MultiQuant v3.0.2 (AB Sciex, Concord, ON, Canada) was used for calibration and chromatographic peak integration. Metabolite abundance was quantified through chromatographic peak area integration [22–27].

2.7. qRT-PCR

Before further processing, all samples were treated using Solid RNase Scavenger (1 part per thousand; Coolaber, Beijing, China). A mortar and pestle were then used to grind storage root samples to a powder in liquid nitrogen, after which RNaiso Plus (Takara Biotechnology, Beijing, China) was employed for RNA extraction. The sample

concentrations were then measured based on A260/A280 ratios using an ultra-low-volume spectrometer (Bio Drop, Cambridge, UK), and a Prime Script™ RT reagent Kit with gDNA Eraser (Takara Biotechnology, Beijing, China) was employed for cDNA preparation using only those samples with an A260/A280 ratio of 1.8–21. After diluting the resultant cDNA samples 5-fold, they were used for qPCR analyses, performed using a Bio-Rad CFX96 Real-Time PCR instrument and TB Green® Premix Ex Taq™ II (Takara Biotechnology, Dalian, China) as follows: 95 °C for 30 s; 40 cycles at 95 °C for 5 s; 60 °C for 30 s. Melt curves (60–95 °C; 0.5 °C increments for 5 s) were used to confirm specificity. Relative gene expression was measured in Bio-Rad Manager 3.1 via the ΔΔCq approach [29], and actin served as the normalization control. Primer Premier 5.0 (Table S1) was utilized for primer design.

2.8. Statistical Analyses

To better standardize the data and improve normality, metabolite data were subjected to logarithmic transformation. PCA (Principal Component Analysis), HCA (hierarchical cluster analysis), and OPLS-DA (Partial Least Squares-Discriminant Analysis analysis) were employed to assess the metabolite profiles using R [22–27]. Unique metabolites present in different sample groups were identified using Venn diagrams. The functions of metabolites that were differentially abundant between the BS and S19 sweet potato cultivars were explored using the KEGG (Kyoto Encyclopedia of Genes and Genomes) database, with $p < 0.01$ as the cut-off for significance. GraphPad Prism v6.01 (GraphPad Software, Inc., San Diego, CA, USA) was used to plot all experimental data. And qRT-PCR was used to analyze gene expression trends between different varieties and to analyze the correlation between gene expression and metabolite content.

3. Results

3.1. Analyses of Total Flavonoid Levels in Sweet Potato Storage Roots

Initially, the phenotypic characteristics of sweet potato storage roots were assessed, revealing no significant changes in the coloration of the yellow-fleshed BS and white-fleshed S19 cultivars over the course of maturation (Figure 2a). Consistently, the total flavonoid content in the BS samples remained 2–3-fold higher than that in the S19 samples throughout the maturation process (S1–S4). For further analyses, samples from the S2 and S4 time points were utilized, with significant differences in total flavonoid content being evident between the BS and S19 cultivars at each of these time points with respect to the total flavonoid content (Figure 2b).

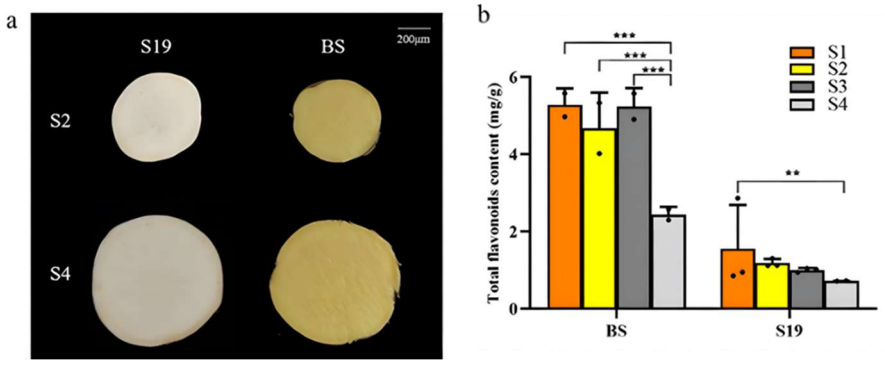

Figure 2. (**a**) Phenotypic characteristics of S19-S2, S19-S4, BS-S2, and BS-S4 storage root samples. (**b**) Total flavonoid content in prepared samples from BS and S19 cultivars. *** $p < 0.001$, ** $p < 0.01$.

3.2. Widely Targeted Metabolomic Analysis of Differential Metabolites

Next, a widely targeted UPLC-MS/MS metabolomics approach was used to characterize the metabolite profiles in the S19-S2, S19-S4, BS-S2, and BS-S4 samples. After filtering, 578 total metabolites were identified, including 71 amino acids and amino acid deriva-

tives, 54 organic acids, 46 nucleotides and nucleotide derivatives, 114 lipids, 28 flavonoids, 1 quinone, 28 lignans and coumarins, 108 phenolic acids, 3 tannins, 48 alkaloids, 9 terpenoids, 1 steroid, and 67 other compounds (Table S2).

Principal Component Analysis (PCA) is a statistical technique that uses several principal components to reveal the overall metabolic differences between groups, as well as the variability between the samples within each group. In this study, two principal components, PC1 and PC2, were extracted, accounting for 32.78% and 16.11% of the total variance, respectively. There was clear separation of the two samples in the PCA score plot (Figure 3a). Cluster heatmaps were further employed to assess the metabolite profiles in these samples, revealing clear clustering among these biological replicates consistent with a high degree of reliability. Flavonoid metabolite analyses additionally revealed higher overall levels of these metabolites in the BS samples compared to the S19 samples, in line with the total flavonoid content results shown above (Figure 3b). OPLS-DA models were next used to further examine metabolite abundance variations among samples based on the filtering of any orthogonal metabolite changes not related to variable classification, thereby maximizing the differences between sample groups to better detect divergent metabolites. Pairwise comparisons between the S19-S2, BS-S2, S19-S4, and BS-S4 samples were performed using the OPLS-DA model to detect differing metabolites among groups (Figure S1), yielding the following model quality parameters indicative of successful modeling: $R^2X = 0.738$, $Q^2 = 0.953$, $R^2Y = 0.996$; $R^2X = 0.0.688$, $Q^2 = 0.955$, $R^2Y = 0.996$. These results were also validated through 200 permutation analyses (Figure S2). Overall, these analyses collectively demonstrated the substantial differences between the samples, together with the strong similarity of the biological replicates and overall good sample repeatability within the study.

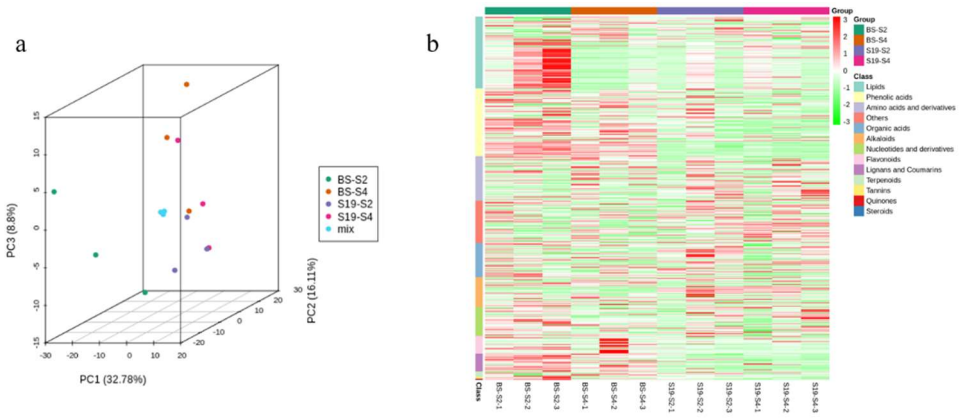

Figure 3. Preliminary analysis of metabolomics data. Principal Component Analysis of metabolites (**a**); Cluster analysis of metabolites (**b**).

3.3. Identification of Differential Flavonoid Metabolites and Their Functional Annotation and Enrichment

A volcano plot provides a quick way to see differences in the levels of metabolites in two samples, as well as the statistical significance of these differences. In total, 214 significantly differentially abundant metabolites were detected for the S19-S2 vs. BS-S2 comparison (156 upregulated, 58 downregulated), while 188 were detected for the S19-S4 vs. BS-S4 comparison (120 upregulated, 68 downregulated) (Figure 4a,b). Differential flavonoid metabolites were identified in the comparison group by combining the fold change and variable importance in projection (VIP) values of the OPLS-DA model. When using VIP $\geq$ 1.0 and $|Log2FC| \geq 1$ as the threshold to define significant differences, for the S19-S2 vs. BS-S2 comparison, 14 significantly differentially abundant flavonoid metabolites were detected, including one isoflavone, one flavonoid carbonoside, five flavonols, two flavonoids, one anthocyanin, one dihydroflavonol, one dihydroflavone, and two chalcones. Similarly, when comparing the S19-S4 and BS-S4 samples, 10 significantly different abundant flavonoid metabolites were identified, including one isoflavone, one flavonoid carbonoside, four flavonols, two flavonoids, one anthocyanin, and one chalcone. (Table S3).

In addition, the KEGG enrichment analysis showed that the S19-S2 vs. BS-S2 and S19-S4 vs. BS-S4 groups were enriched in the flavone and flavonol biosynthesis pathway and the flavone biosynthesis pathway (Figure 4c,d, Table S4).

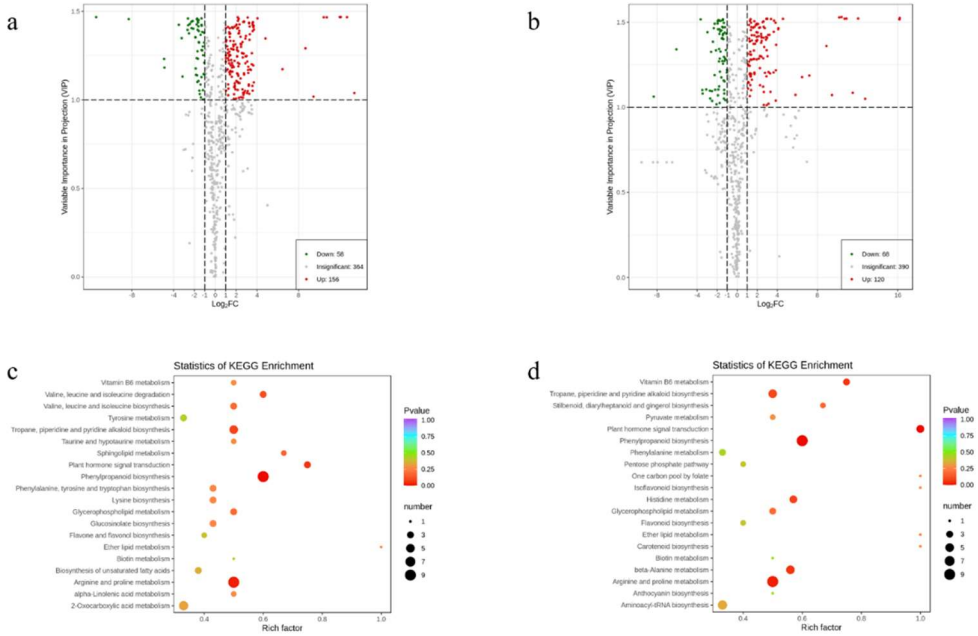

Figure 4. Volcano plots for S19-S2 vs. BS-S2 and S19-S4 vs. BS-S4 (**a**,**b**), KEGG pathway enrichment for S19-S2 vs. BS-S2 and S19-S4 vs. BS-S4 (**c**,**d**).

3.4. qRT-PCR

Flavonoid biosynthesis is an extremely complex pathway that entails the phenylpropane synthesis pathway and a range of secondary pathways including the flavonoid and anthocyanin metabolic pathways. To more fully explore the molecular basis for the observed differences in flavonoid- and flavor-related metabolites in these samples, qPCR analysis was next used to profile the expression of key flavonoid metabolism-related genes (Figure 5). The expression of *PAL*, *C4H*, *4CL*, *CHS*, *CHI*, *IFS*, *F3H*, *F3′H*, *DFR*, *ANS*, *ANR*, *FLS*, *UTG*, and *FNS* in BS was higher than that in S19, and the difference between *PAL* and *F3′H* levels was the most significant. In BS-S2 and BS-S4, the *PAL* expression levels were 10.98 and 4.15 times that of S19, and *F3′H* expression levels were 3.38 and 6.93 times that of S19, respectively, while the expression of both *PAL* and *F3′H* decreased with the expansion of sweet potato root, which was consistent with the phenotypic data. However, the expression level of *FLS* was completely opposite to the phenotype (Figure 2a). The expression level of S19 in S2 and S4 was higher than that of BS, which was increased by 4.76 times and 20.66 times, respectively.

3.5. Flavonoid Biosynthesis Regulatory Network

To better understand the relationships between metabolites and genes in flavonoid biosynthesis, the combination of metabolites and genes in a network can more intuitively show the relationship between gene expression and metabolite content (Figure 6). *IbPAL*, *IbF3′H*, and *IbFNS*, which showed significant expression differences, were highly expressed in BS, and *IbFLS* was highly expressed in S19. The BS and S19 metabolites associated with flavonoid biosynthesis are flavonoid carbonoside, flavonols, flavonoids, anthocyanins, dihydroflavonol, dihydroflavone, chalcones, and isoflavones. Of these, the most marked difference in flavonoids was between naringenin and *IbFNS* catalysis, which was 7.90 times the level of flavonoid expression of S19 in S4, compared with BS. It was also observed that during this period, the kaempferol-4′-o-glucoside, 5,2′,5′-trihydroxy-3,7,4′-trimethoxyflavone-2′-o-glucoside, luteolin-6-C-glucoside-7-O-(6″-fer arabinoside,

and eriodictyol-7-O-glucoside contents of uloyl were also higher than those in S19. However, the content of eriodictyol-7-O-glucoside was significantly higher in BS than that in S19. The expression level and metabolite content of *IbFLS* in S19-S4 was higher than that in BS. The main metabolites were kaempferol-3-O-galactoside (Trifolin), Kaempferol-3-O-glucoside (Astragalin), Quercetin-7-O-glucoside*, Kaempferol-3-O-(2″-o-acetyl) glucuronide, and kaempferol-7-O-glucoside*. It is worth noting that only one metabolite, amoenin, was extremely abundant in BS-S4. However, while the expression levels of *IbPAL* and *IbF3′H* in BS were significantly higher than those in S19, no corresponding metabolites were detected. This may be due to the accumulation of more substrates upstream of Flavonoid synthesis for the synthesis of kaempferol and quercetin, which also indicates that S19 is white in flesh.

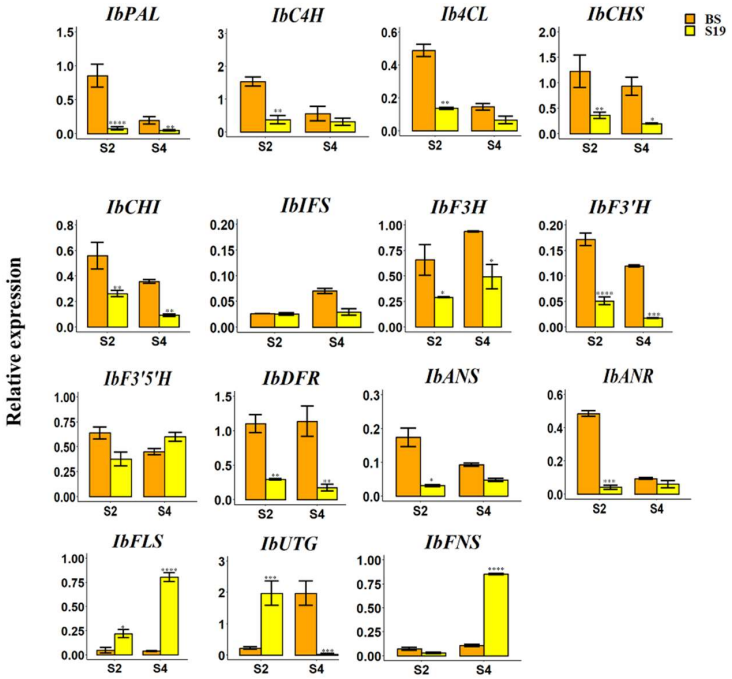

Figure 5. Flavonoid biosynthesis-related gene expression. **** $p < 0.0001$, *** $p < 0.001$, ** $p < 0.01$, * $p < 0.05$.

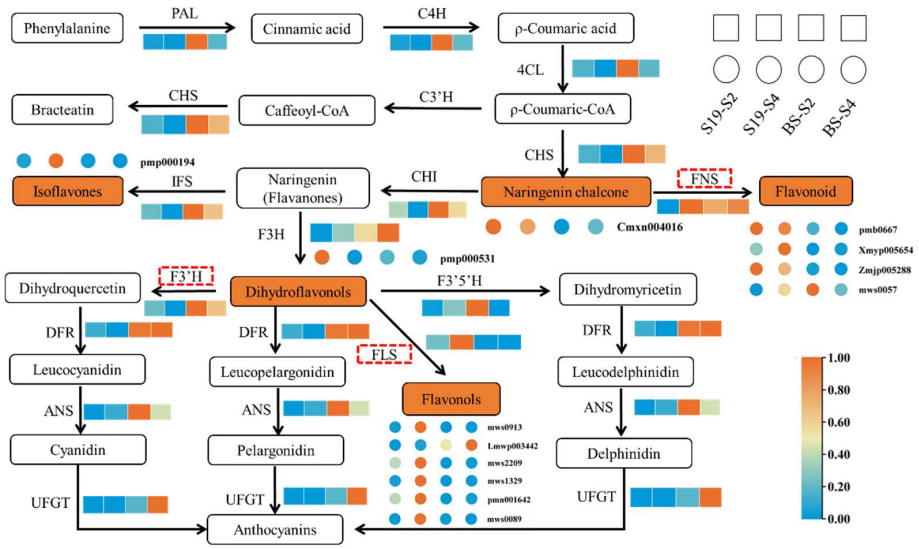

Figure 6. Differential metabolites associated with flavonoid biosynthesis and the gene expression network map (S19-S2, S19-S4, BS-S2, and BS-S4).

4. Discussion

Sweet potatoes are widely cultivated owing to the high nutritional value of both the aboveground and storage root portions of these plants [30]. Flavonoids are key antioxidants and nutritional compounds present within sweet potatoes, offering a range of health benefits [30]. Total flavonoid content is also closely associated with the color of the flesh of sweet potato storage roots, which are rich in pigments, including carotenoids [31] and flavonoids [32]. In prior studies of carotenoids, the most abundantly detected within BS storage roots was β-cryptoxanthin [33]. In contrast, less is known regarding the flavonoid content in sweet potato roots, with most studies to date instead having examined sweet potato leaves [34–36]. To address this knowledge gap, the flavonoid content in the storage roots of the yellow-fleshed BS and white-fleshed S19 sweet potato varieties was assessed, revealing significantly increased flavonoid levels in the BS storage roots compared to the S19 storage roots.

Genes associated with flavonoid biosynthesis have previously been characterized in species including rice [6], maize [7], and ginkgo [37]. The mechanisms underlying flavonoid biosynthesis in sweet potato plants, however, remain to be fully clarified. Here, a combination of widely targeted metabolomics and qPCR analyses was conducted in an effort to more fully understand this biosynthetic process. *PAL*, *C4H*, and *4CL* generate p-coumaroyl-CoA through a series of catalytic reactions, known as the general phenylpropane pathway [8]. In this process, the gene expression levels in BS were significantly higher than those in S19, indicating that BS accumulated a large number of substrates for subsequent reactions. Similarly, the expression of *CHS* was higher in BS and as its catalytic product chalcone is an important yellow pigment in plants, the phenotype of BS was yellow. However, the product of *F3H*, dihydroflavonol, acts as an important branching point in the flavonoid synthesis pathway [38]. It is reported that *FLS* and *DFR* compete for the common substrate dihydroflavonol to regulate the accumulation of flavonols and anthocyanins [39]. Combining the analysis of gene expression and metabolite contents, it was found that *FLS* was highly expressed in S19, and the detected metabolites were all catalytic products of *FLS*. It can be seen that in S19, when dihydroflavonols were used as substrates, the formation of flavonol branches was more likely. Flavonol synthase (FLS), a key enzyme in flavonol biosynthesis, catalyzes the production of kaempferol and myricetin by dihydrokaempferol and dihydromyricetin, respectively. The loss or altered expression of *FLS* can affect the color of plant organs [40,41]. Interestingly, *F3′H* was significantly upregulated in BS storage roots, whereas *FLS* expression was diametrically opposed to that of *F3′H*. The heterologous overexpression of *FLS* in tobacco promotes flavonol biosynthesis [42]. The high *FLS* expression in S19 resulted in increased levels of kaempferol and quercetin derivatives. *FLS* is more active in catalyzing dihydrokaempferol than *F3′H* [42], leading to the accumulation of kaempferol and quercetin derivatives in S19. The content of dihydroflavonol products detected in S19 was significantly higher than that in BS. In addition, studies have shown that the metabolites synthesized by *IbFLS* and *IbFNS* range from colorless to light yellow [13], which also explains the high expression levels of *IbFLS* and *IbFNS* in S19.

5. Conclusions

In summary, the dynamics of flavonoid biosynthesis and flavor-related compound production were herein characterized over the course of maturation in the BS and S19 sweet potato cultivars through a widely targeted metabolomics approach. Metabolomics analysis resulted in the identification of 16 flavonoid metabolites in BS and S19, among which S19 accumulated large amounts of kaempferol and quercetin derivatives, indicating that *IbFLS* was strongly expressed in S19 and participated in the formation of the white S19 flesh. The qRT-PCR results showed that the expression levels of 15 key genes related to flavonoid synthesis, apart from *IbFLS* and *IbFNS*, were upregulated in BS, contributing to the yellow color of BS. However, the high expression of *IbFLS* and *IbFNS* in S19 was found to be interdependent with the corresponding metabolite content, which is consistent with

the metabolite group results, and is also the reason why S19 appears white. Overall, these findings have important implications for the biosynthesis of flavonoids in sweet potatoes.

Supplementary Materials: The following supporting information can be downloaded at: https://www.mdpi.com/article/10.3390/agriculture13101955/s1, Figure S1: Grouped principal component analysis diagram. S19-S2vsBS-S2 (a), S19-S4vs BS-S4 (b). Figure S2: OPLS-DA verification diagram. S19-S2vsBS-S2 (a), S19-S4vs BS-S4 (b). Table S1 qRT-PCR primer design. Table S2 Targeted metabolites in the taproot of sweet potato. Table S3 Significantly different flavonoid metabolites. Table S4 Metabolite statistics of different comparison groups.

Author Contributions: Conceptualization, X.Z.; methodology, B.Z.; software, Y.H.; validation, H.G., Q.D., Q.R. and L.D.; formal analysis, Y.H.; investigation, Q.D.; resources, Y.Z.; data curation, H.G.; writing—original draft preparation, H.G.; writing—review and editing, X.Z.; visualization, H.G.; supervision, H.G.; project administration, H.G.; funding acquisition, H.G. All authors have read and agreed to the published version of the manuscript.

Funding: This research was funded by the Ministerial and Provincial Co-Innovation Center for Endemic Crops Production with High-quality and Efficiency in Loess Plateau (grant number SBGJXTZX-13); the High-level Foreign Experts Introduction Project of China (grant number G2022004009L); the Shanxi Key Laboratory of Minor Crops Germplasm Innovation and Molecular Breeding, Shanxi Agricultural University (grant number 202204010910001); and the Grand Science; Technology Special Project of Shanxi Province (grant numbers 202101140601027) and the Innovation Programs of Graduate Education in Shanxi (23143S0201008).

Data Availability Statement: Not applicable.

Conflicts of Interest: The authors declare no conflict of interest.

References

1. Zhang, L.; Gao, Y.; Deng, B.; Ru, W.; Tong, C.; Bao, J. Physicochemical, Nutritional, and Antioxidant Properties in seven sweet potato flours. *Front. Nutr.* **2022**, *9*, 923257. [CrossRef] [PubMed]
2. Laveriano-Santos, E.P.; López-Yerena, A. Jaime-Rodríguez, C.; González-Coria, J.; Lamuela-Raventós, R.M.; Vallverdú-Queralt, A.; Romanyà, J.; Pérez, M. Sweet potato is not simply an abundant food crop: A Comprehensive Review of Its Phytochemical Constituents, Biological Activities, and the Effects of Processing. *Antioxidants* **2022**, *11*, 1648. [PubMed]
3. Parveen, A.; Choi, S.; Kang, J.H.; Oh, S.H.; Kim, S.Y. Trifostigmanoside I, an Active Compound from Sweet Potato, Restores the Activity of MUC2 and Protects the Tight Junctions through PKCα/β to Maintain Intestinal Barrier Function. *Int. J. Mol. Sci.* **2020**, *22*, 291. [CrossRef] [PubMed]
4. Gou, S.; Zhang, X.; Han, W.; Li, Q.; Li, X. Research Progress on the Biosynthesis and Antistress Mechanisms of Plant Flavonoids. *J. Hortic. Sci.* **2023**, *50*, 209–224.
5. Zhang, K.; Sun, Y.; Li, M.; Long, R. CrUGT87A1, a UDP-sugar glycosyltransferases (UGTs) gene from Carex rigescens, increases salt tolerance by accumulating flavonoids for antioxidation in Arabidopsis thaliana. *Plant Physiol. Biochem.* **2021**, *159*, 28–36.
6. Lam, P.Y.; Wang, L.; Lui, A.C.W.; Liu, H.; Takeda-Kimura, Y.; Chen, M.X.; Zhu, F.Y.; Zhang, J.; Umezawa, T.; Tobimatsu, Y.; et al. Deficiency in flavonoid biosynthesis genes CHS, CHI, and CHIL alters rice flavonoid and lignin profiles. *Plant Physiol.* **2022**, *188*, 1993–2011.
7. Peniche-Pavía, H.A.; Guzmán, T.J.; Magaña-Cerino, J.M.; Gurrola-Díaz, C.M.; Tiessen, A. Maize Flavonoid Biosynthesis, Regulation, and Human Health Relevance: A Review. *Molecules* **2022**, *27*, 5166. [CrossRef]
8. Dong, N.Q.; Lin, H.X. Contribution of phenylpropanoid metabolism to plant development and plant-environment interactions. *J. Integr. Plant Biol.* **2020**, *63*, 180–209.
9. Lin, S.; Singh, R.K.; Moehninsi, M.; Navarre, D.A. R2R3-MYB transcription factors, StmiR858 and sucrose mediate potato flavonol biosynthesis. *Hortic. Res.* **2021**, *8*, 25.
10. Meng, X.; Li, Y.; Zhou, T.; Sun, W.; Shan, X.; Gao, X.; Wang, L. Functional Differentiation of Duplicated Flavonoid 3-O-Glycosyltransferases in the Flavonol and Anthocyanin Biosynthesis of *Freesia hybrida*. *Front. Plant Sci.* **2019**, *10*, 1330.
11. LaFountain, A.M.; Yuan, Y.W. Repressorsof anthocyanin biosynthesis. *New Phytol.* **2021**, *231*, 933–949. [CrossRef] [PubMed]
12. Wang, F.; Wang, X.J.; Zhao, S.N.; Yan, J.R.; Bu, X.; Zhang, Y.; Liu, Y.F.; Xu, T.; Qi, M.F.; Qi, H.Y.; et al. Light Regulation of Anthocyanin Biosynthesis in Horticultural Crops. *Sci. Agric. Sin.* **2020**, *53*, 4904–4917.
13. Shen, N.; Wang, T.; Gan, Q.; Liu, S.; Wang, L.; Jin, B. Plant flavonoids: Classification, distribution, biosynthesis, and antioxidant activity. *Food. Chem.* **2022**, *383*, 132531. [PubMed]
14. Chen, C.; Zhang, Y.; Fu, X.; Chen, C.; Wu, S.; Zhang, C.; Zhang, H.; Chang, Y.; Chen, S.; Zhao, J.; et al. Influential factors and transcriptome analyses of immature diploid embryo anthocyanin accumulation in maize. *BMC. Plant. Biol.* **2022**, *22*, 609.

15. Lv, L.; Chen, X.; Li, H.; Huang, J.; Liu, Y.; Zhao, A. Different adaptive patterns of wheat with different drought tolerance under drought stresses and rehydration revealed by integrated metabolomic and transcriptomic analysis. *Front. Plant. Sci.* **2022**, *13*, 1008624.
16. Chen, X.; Yang, Y.; Yang, X.; Zhu, G.; Lu, X.; Jia, F.; Diao, B.; Yu, S.; Ali, A.; Zhang, H.; et al. Investigation of flavonoid components and their associated antioxidant capacity in different pigmented rice varieties. *Food. Res. Int.* **2022**, *161*, 111726. [CrossRef]
17. Hall, R.D.; Brouwer, I.D.; Fitzgerald, M.A. Plant metabolomics and its potential application for human nutrition. *Physiol. Plant* **2008**, *132*, 162–175. [CrossRef]
18. Zhou, J.; Hou, D.; Zou, W.; Wang, J.; Luo, R.; Wang, M.; Yu, H. Comparison of Widely Targeted Metabolomics and Untargeted Metabolomics of Wild Ophiocordyceps sinensis. *Molecules* **2022**, *27*, 3645. [CrossRef]
19. Yang, X.; Zhao, X.; Fu, D.; Zhao, Y. Integrated Analysis of Widely Targeted Metabolomics and Transcriptomics Reveals the Effects of Transcription Factor NOR-like1 on Alkaloids, Phenolic Acids, and Flavonoids in Tomato at Different Maturation Stages. *Metabolites* **2022**, *12*, 1296. [CrossRef]
20. Chen, W.; Gong, L.; Guo, Z.; Wang, W.; Zhang, H.; Liu, X.; Yu, S.; Xiong, L.; Luo, J. A novel integrated method for large-scale detection, identification, and quantification of widely targeted metabolites: Application in the study of rice metabolomics. *Mol. Plant.* **2013**, *6*, 1769–1780. [CrossRef]
21. Wang, A.; Li, R.; Ren, L.; Gao, X.; Zhang, Y.; Ma, Z.; Ma, D.; Luo, Y. A comparative metabolomics study of flavonoids in sweet potato with different flesh colors (*Ipomoea batatas* (L.) Lam). *Food Chem.* **2018**, *260*, 124–134. [PubMed]
22. Eriksson, E.J.L.; Kettaneh-Wold, N.; Trygg, J.; Wikström, C.; Wold, S. *Multi- and Megavariate Data Analysis, Part I—Basic Principles and Applications*, 2nd ed.; Umetrics Academy: Stockholm, Sweden, 2006.
23. Chen, Y.; Zhang, R.; Song, Y.; He, J.; Sun, J.; Bai, J.; An, Z.; Dong, L.; Zhan, Q.; Abliz, Z. RRLC-MS/MS-based metabonomics combined with in-depth analysis of metabolic correlation network: Finding potential biomarkers for breast cancer. *Analyst* **2009**, *134*, 2003–2011. [CrossRef] [PubMed]
24. Thévenot, E.A.; Roux, A.; Xu, Y.; Ezan, E.; Junot, C. Analysis of the Human Adult Urinary Metabolome Variations with Age, Body Mass Index, and Gender by Implementing a Comprehensive Workflow for Univariate and OPLS Statistical Analyses. *J. Proteome Res.* **2015**, *14*, 3322–3335. [PubMed]
25. Kanehisa, M.; Goto, S. KEGG: Kyoto encyclopedia of genes and genomes. *Nucleic. Acids. Res.* **2000**, *28*, 27–30. [CrossRef] [PubMed]
26. Chong, J.; Xia, J. MetaboAnalystR: An R package for flexible and reproducible analysis of metabolomics data. *Bioinformatics* **2018**, *34*, 4313–4314. [CrossRef]
27. Noguchi, A.; Nakamura, K.; Sakata, K.; Sato-Fukuda, N.; Ishigaki, T.; Mano, J.; Takabatake, R.; Kitta, K.; Teshima, R.; Kondo, K.; et al. Development and interlaboratory validation of a simple screening method for genetically modified maize using aΔΔC(q)-based multiplex real-time PCR assay. *Anal. Chem.* **2016**, *88*, 4285–4293. [CrossRef]
28. Yang, C.; Luo, J. Establishment and research of method for determination of total flavonoid content of oily hemp blood vine in Guizhou. *Guizhou Sci.* **2022**, *40*, 11–14.
29. Nguyen, H.C.; Chen, C.C.; Lin, K.H.; Chao, P.Y.; Lin, H.H.; Huang, M.Y. Bioactive Compounds, Antioxidants, and Health Benefits of Sweet Potato Leaves. *Molecules* **2021**, *26*, 1820. [CrossRef]
30. Althwab, S.A.; Mousa, H.M.; El-Zaha, K.M.; Zaher, A.M.A. Protective effect of sweet potato peel against oxidative stress in hyperlipidemic albino rats. *Food Nutr. Sci.* **2019**, *10*, 503–516. [CrossRef]
31. Kang, L.; Park, S.C.; Ji, C.Y.; Kim, H.S.; Lee, H.S.; Kwak, S.S. Metabolic engineering of carotenoids in transgenic sweetpotato. *Breed. Sci.* **2017**, *67*, 27–34.
32. Zhou, W.; Gong, Y.; Lu, X.; Huang, C.; Gao, F. Molecular cloning and characterization of a flavonoid 3′-hydroxylase gene from purple-fleshed sweet potato (*Ipomoea batatas*). *Mol. Biol. Rep.* **2012**, *39*, 295–302. [CrossRef] [PubMed]
33. Ren, Q.; Zhen, X.; Gao, H.; Liang, Y.; Li, H.; Zhao, J.; Yin, M.; Han, Y.; Zhang, B. Integrated Metabolomic and Transcriptomic Analyses Reveal the Basis for Carotenoid Biosynthesis in Sweet Potato (*Ipomoea batatas* (L.) Lam.) Storage Roots. *Metabolites* **2022**, *12*, 1010. [CrossRef] [PubMed]
34. Gao, X.R.; Zhang, H.; Li, X.; Bai, Y.W.; Peng, K.; Wang, Z.; Dai, Z.R.; Bian, X.F.; Zhang, Q.; Jia, L.C.; et al. The B-box transcription factor IbBBX29 regulates leaf development and flavonoid biosynthesis in sweet potato. *Plant Physiol.* **2023**, *191*, 496–514.
35. Zhang, Y.; Bian, S.; Hu, J.; Liu, G.; Peng, S.; Chen, H.; Jiang, Z.; Wang, T.; Ye, Q.; Zhu, H. Natural Deep Eutectic Solvent-Based Microwave-Assisted Extraction of Total Flavonoid Compounds from Spent Sweet Potato (*Ipomoea batatas* L.) Leaves: Optimization and Antioxidant and Bacteriostatic Activity. *Molecules* **2022**, *27*, 5985. [CrossRef]
36. Li, G.; Lin, Z.; Zhang, H.; Liu, Z.; Xu, Y.; Xu, G.; Li, H.; Ji, R.; Luo, W.; Qiu, Y.; et al. Anthocyanin Accumulation in the Leaves of the Purple Sweet Potato (*Ipomoea batatas* L.) Cultivars. *Molecules* **2019**, *24*, 3743. [CrossRef] [PubMed]
37. Liu, X.G.; Wu, S.Q.; Li, P.; Yang, H. Advancement in the chemical analysis and quality control of flavonoid in Ginkgo biloba. *J. Pharm. Biomed. Anal.* **2015**, *113*, 212–225.
38. Tang, Y.; Cai, W.; Xu, B. Profiles of phenolics, carotenoids and antioxidative capacities of thermal processed white, yellow, orange and purple sweet potatoes grown in Guilin, China. *Food Sci. Hum. Wellness* **2015**, *4*, 123–132. [CrossRef]
39. Lou, Q.; Liu, Y.L.; Qi, Y.Y.; Jiao, S.Z.; Tian, F.F.; Jiang, L.; Wang, Y.J. Transcriptome sequencing and metabolite analysis reveals the role of delphinidin metabolism in flower color in grape hyacinth. *J. Exp. Bot.* **2014**, *65*, 3157–3164. [CrossRef]

40. Takahashi, R.; Githiri, S.M.; Hatayama, K.; Dubouzet, E.G.; Shimada, N.; Aoki, T.; Ayabe, S.; Iwashina, T.; Toda, K.; Matsumura, H. A single-base deletion in soybean flavonol synthase gene is associated with magenta flower color. *Plant. Mol. Biol.* **2007**, *63*, 125–135. [CrossRef]
41. Nielsen, K.; Deroles, S.C.; Markham, K.R.; Bradley, M.J.; Podivinsky, E.; Manson, D. Antisense flavonol synthase alters copigmentation and flower color in lisianthus. *Mol. Breed.* **2002**, *9*, 217–229. [CrossRef]
42. Lin, Q.F.; Liu, T.T.; Liu, J.R.; Cai, M.; Cheng, T.R.; Wang, J.; Zhang, Q.X.; Pan, H.T. Flavonoids composition and content in petals of Lagerstroemia and Heimia species and cultivars. *Acta Hortic. Sin.* **2021**, *48*, 1956–1968.